Remote Sensing of Environment 274 (2022) 112981

Contents lists available at ScienceDirect

Remote Sensing of Environment

journal homepage: www.elsevier.com/locate/rse

A novel identification method for unrevealed mesoscale eddies with transient and weak features-Capricorn Eddies as an example

Li Zhibing [a,b,c], Cai Zhongya [d], Liu Zhiqiang [b,*], Wang Xiaohua [c,e], Hu Jianyu [f]

[a] Southern Marine Science and Engineering Guangdong Laboratory (Guangzhou), Guangzhou, China
[b] Department of Ocean Science and Engineering, Southern University of Science and Technology, Shenzhen, China
[c] The Sino-Australian Research Consortium for Coastal Management, The University of New South Wales, Canberra, ACT, Australia
[d] State Key Laboratory of Internet of Things for Smart City and Department of Civil and Environmental Engineering, University of Macau, Macau, China
[e] School of Science, The University of New South Wales, Canberra, ACT, Australia
[f] State Key Laboratory of Marine Environmental Science, College of Ocean and Earth Sciences, Xiamen University, Xiamen 361102, China

ARTICLE INFO

Editor: Menghua Wang

Keywords:
Eddy identification
Capricorn eddies
Interannual variability

ABSTRACT

Traditional eddy detection methods can well identify eddies with long lifespans (usually >4 weeks) and strong hydrographic features. Eddies with shorter lifespans or intermittent features are arduous to detect and might be eliminated or misclassified during the detection. However, these eddies have been reported as a majority of the mesoscale eddies in global oceans. This study developed a novel eddy identification method for those eddies. Different from the traditional eddy detection performed based on a snapshot of observations in the horizontal plane, this novel identification method was developed on the evolution of eddies in the temporal dimension. It efficiently avoids the failure in detecting eddies with inconspicuous features during some stages of their evolutions and also eliminates excessive detection. The developed method was implemented to detect Capricorn Eddies based on 26 years of sea-level anomaly from satellite altimetry. Capricorn Eddies are transient and intermittent phenomena induced as a result of the East Australian Current colliding with the continental shelf edge near the Fraser Island, Australia. Using the new identification method, the characteristics of Capricorn Eddies, including their temporal and spatial scales, intensity preferences and evolution details, were resolved. Remarkable seasonal variations of the Capricorn Eddies were also revealed. Based on these findings, a comprehensive overview of Capricorn Eddies, which is crucial for further understanding the variabilities of regional biogeochemical processes and ocean ecosystems, was provided. The developed method will also provide potential insight into the unrevealed eddies in the global oceans.

1. Introduction

Mesoscale eddies are ubiquitous phenomena in the ocean. They are crucial in modulating the cross-scale energy transfer and thereby ocean mixing and primary productivity (Chelton et al., 2011; Gaube et al., 2013). Variations of the primary productivity subsequently affect the predators' distributions and their behavioral decisions. For instance, the mesoscale eddies are important offshore foraging grounds for seabirds (Weimerskirch et al., 2004; Cotté et al., 2007), pinnipeds (Bailleul et al., 2010; Dragon et al., 2010) and cetaceans (Sims and Quayle, 1998; Woodworth et al., 2012). However, some eddies have transient or weak hydrographic features due to their low intensity or the interactions with surrounding water, which makes these eddies are arduous to be well detected.

Cyclonic eddies (Capricorn Eddies) located in the gap between the Southern Great Barrier Reef (SGBR) and the Fraser Island (Fig. 1) have been observed since 1960s (Woodhead, 1970; Griffin et al., 1987; Kleypas and Burrage, 1994; Weeks et al., 2010). Capricorn eddies have been identified as an important influence on variability of regional marine ecosystems but with transient features (Weeks et al., 2010; Mao and Luick, 2014). Organisms brought by the Capricorn Eddies feed the fish, turtles, scallops, and seabirds, making this area massively productive (Weeks et al., 2010). For example, Manta rays travel hundreds of kilometers to forage offshore, specifically in the ocean where Capricorn Eddies are observed (Jaine et al., 2014). Weeks et al. (2010) concluded that Capricorn Eddies have a critical effect on raising and transporting nutrient-rich water to support the ecosystem.

Woodhead (1970) proposed the possible presence of a cyclonic eddy

* Corresponding author.
E-mail address: liuzq@sustech.edu.cn (L. Zhiqiang).

https://doi.org/10.1016/j.rse.2022.112981
Received 21 July 2021; Received in revised form 26 February 2022; Accepted 28 February 2022
Available online 17 March 2022

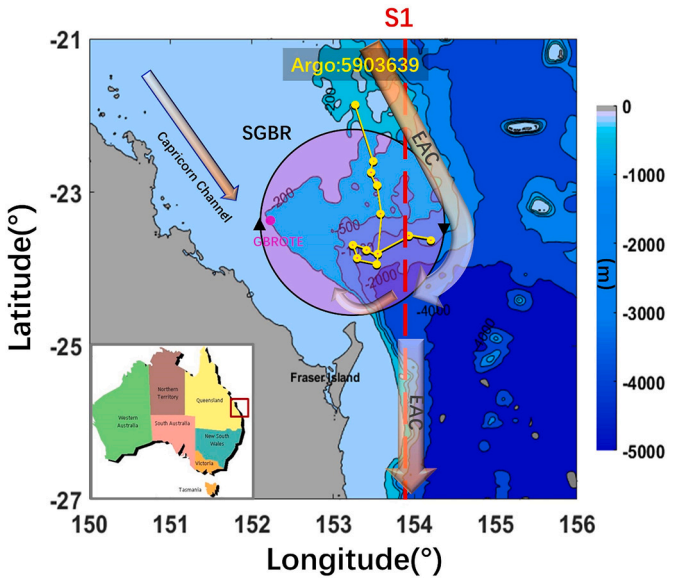

Fig. 1. Geographic location of the Capricorn Eddies (pink circle with black arrow edge). Orange arrows indicate the East Australian Current (EAC), its branch in the Capricorn Channel and bifurcation off the Fraser Island (Weeks et al., 2010). Yellow points and lines are the locations and path of the Argo 5903639 (www.argo.ucsd.edu/About_Argo.html), respectively, used to validate the study. S1 (the dashed red line) is the selected section for the case study demonstration. The pink dot is a mooring site (GBROTE). (For interpretation of the references to colour in this figure legend, the reader is referred to the web version of this article.)

in the gap between the SGBR and Fraser Island after observing a northwestward current inside the Capricorn Channel. Griffin et al. (1987) analyzed the low-frequency component of the northward flow at mouth of the Capricorn Channel using current meters and suggested that this could be a result of a large cyclonic eddy. Kleypas and Burrage (1994) later collected two-year sea surface temperature (SST) images which further supported these results (Woodhead, 1970; Griffin et al., 1987), and concluded that cyclonic eddies are subsistent and possibly correlated to the bifurcation of the East Australian Current (EAC). Burrage et al. (1996) detected satellite remote sensed SST images for a four-year period and achieved a similar result, in which cyclonic eddies were found to occur occasionally during the studied period. They also suggested that pulses of the EAC intensity and pathway are important for the generation of cyclonic eddies. These cyclonic eddies were named Capricorn Eddies. The EAC off the New South Wales coast has obvious seasonal (Ridgway and Godfrey, 1997; Ridgway and Hill, 2009), interannual to decadal (Holbrook et al., 2005, 2011; Yang et al., 2016, 2020) variations, which may provide a hint of the corresponding seasonal or interannual variation of the eddies. Weeks et al. (2010) examined the Capricorn Eddies using satellite remote sensing, in-situ measurements, and numerical simulations in order to explain the dynamical processes during the presence of a cyclonic eddy, such as the upwelling of cooler and nutrient-rich waters onto the shelf. Mao and Luick (2014) explored ocean circulation in the SGBR and found a collision between the EAC and the shelf edge near the Fraser Island. The EAC flowing along the SGBR is regarded as the main energy source for the generation of Capricorn Eddies (Weeks et al., 2010; Mao and Luick, 2014). However, the regional circulation regulating the Capricorn Eddies is complicated and paradoxical. When the EAC flows closely along the continental slope, it will encounter the continental shelf edge before arriving the Fraser Island, causing a flow to be bifurcated from the EAC to form a southward cyclonic flow (Capricorn Eddies). When the Capricorn Eddies grow, they push the EAC away from the continental shelf and prevent the attachment of the EAC from the shelf edge. As a result, the increscent Capricorn Eddies cut their own support. Furthermore, a branch of the EAC intrusion into the Great Barrier Reef flows along the coast and out of the Capricorn Channel (Andrews and Furnas, 1986; Brinkman et al., 2001). However, the branched flow is a negative factor in the Capricorn Eddies' evolution, because if the outflow from the Capricorn Channel is strong, it will depress the Capricorn Eddies' generation or diminish the Capricorn Eddies. Nevertheless, southerly winds can reverse the outflow from the Capricorn Channel and thus facilitate the appearance of Capricorn eddies (Mao and Luick, 2014). These controllers jointly determine the characteristics of the Capricorn Eddies. For instance, the variable temporal scales of the controllers may lead to different lifespans of the Capricorn Eddies from days to months.

As the previous studies only probed individual cases and summarized one-sided features, a comprehensive understanding of the Capricorn Eddies' spatiotemporal variability is still lacking. For instance, no census of their lifespans, spatial scales, evolutions and long-term variations is available because of a lack of consecutive observational data. As mentioned previously, the occurrences of the local eddies may only last for days which made the eddies hard to be detected. Therefore, to address these questions and provide a comprehensive understanding, we audited the Capricorn Eddies using a new detection method based on 26 years of satellite altimeter observations and the known water properties. The method can provide reliable detections for both the cyclonic and anti-cyclonic eddies in this region.

The altimeter data provide a wealth of information for probing mesoscale eddies. Eddy detection has become feasible in the recent decades by using widely implemented satellite altimeter data. Subsequently, many detection methods have been developed for the physical or geometrical features of eddies. The Okubo-Weiss method (Okubo, 1970; Weiss, 1991) is a physical parameter-based method that has been widely adopted. However, this method may not be feasible to detect some weak eddies without mature structures to be resolved by the empirical parameters and give fake vortices (Chelton et al., 2007; Henson and Thomas, 2008). The winding-angle approach was proposed by Sadarjoen and Post (2000) to identify clustering closed or spiral streamlines. It is sensitive to both weak and intense eddies and requires tuning specific geometric parameters (Yi et al., 2014). Later, Nencioli et al. (2010) updated this method to a pure geometric-velocity-based algorithm, which was further implemented and improved by Williams et al. (2011), Liu et al. (2012) and Müller et al. (2017). These methods all require the fine-tuning of parameters to perform well. Meanwhile, a series of methods based on the observed maps of sea surface height have also been developed and widely accepted as less pre-settlement is required for detection (Chaigneau and Pizarro, 2005; Chelton et al., 2011; Fang and Morrow, 2003; Peaven, 2011; Wang et al., 2003).

These algorithms can detect eddies with circular shapes or strong physical features at a single time. Most algorithms also have a common requirement for eddy tracking, which assumes that the shape of an eddy does not change significantly as it propagates. However, eddies neighboring with each other may have similar shapes, which handicaps tracking of eddies. Alternatively, some eddies may disappear at the surface during their evolutions (Chelton et al., 2011), which is problematic for the detection and tracking methods. For example, short-lived eddies (less than 30 days), which have been identified as a large proportion of the total eddies in the global oceans (> 60%; Chen and Han, 2019), are mostly unstable and have weaker hydrodynamic features, making them difficult to be detected. Fig. 2 shows the schematic plots of possible cases that eddy-detection methods may encounter, as summarized in previous studies. We listed three detection methods to illustrate their behavior in these cases. Case ① is a propagating eddy with a circular shape and clear surface features (Fig. 2a) during its evolution. The sea level anomaly (SLA) threshold method, Okubo-Weiss method (OW), and hybrid method (HD), which combines the SLA-based method and OW method, all have nearly 100% successful detection rates in this case, as mentioned in previous studies (Faghmous et al., 2015; Yi et al., 2014). This indicates that the current detection methods can resolve the eddies well, as in Case ①. However, when an eddy has a transient or

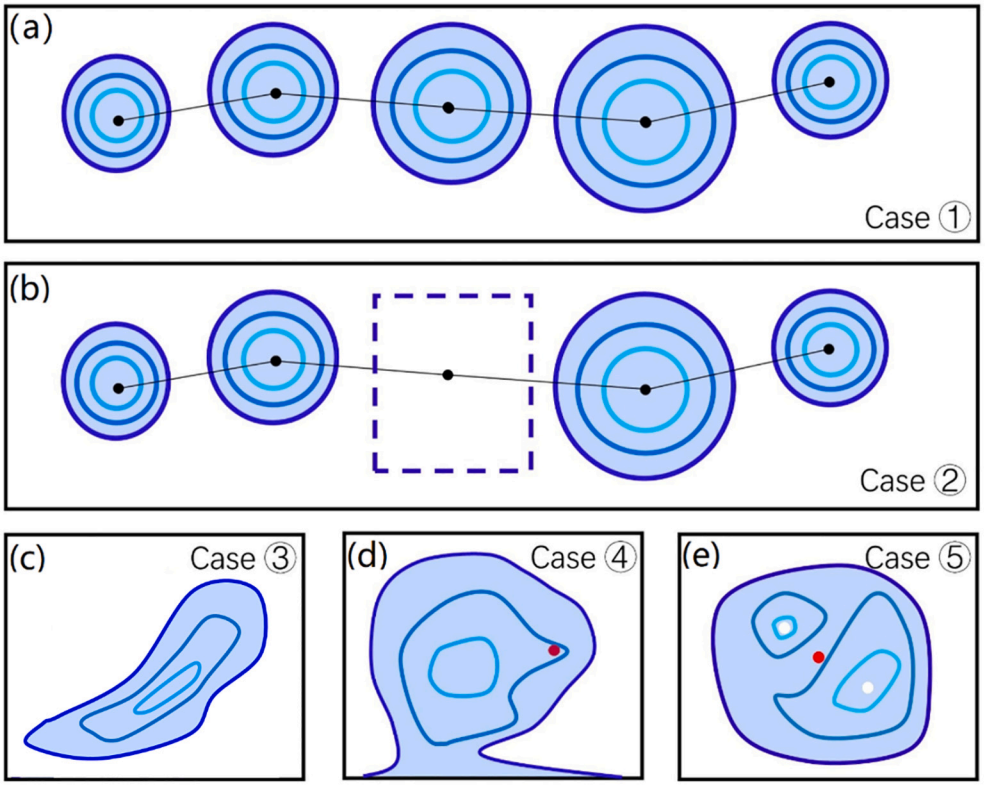

Fig. 2. Five cases for eddy detection and tracking. (a) Case ①: a propagating eddy with clear surface and strong physical features; (b) Case ②: a propagating eddy that temporally loses its surface appearance. The period is longer than the allocated pre-set tracking time intervals; (c) Case ③: an eddy with irregular-circle shape; (d) Case ④: an eddy with spiral streamlines on one side; and (e) Case ⑤: multiple core eddies. White spots denote real eddy cores. Red spots denote fake eddy cores. (For interpretation of the references to colour in this figure legend, the reader is referred to the web version of this article.)

inconspicuous feature (Case ②), for example, the inconspicuous surface lasts longer than the pre-setting detecting and tracking time-steps, almost all these methods fail the detection (Fig. 2b) and tracking procedure. Thus, the missing detection rates (MDRs) were very high in this case. These detection methods eventually break the original eddy into two by mistake, which increases the total eddy numbers and reduces the eddy lifespans. Cases ③, ④, and ⑤ are the cases that these eddy detection methods will encounter but cannot handle well. An eddy with irregular-circle shape (Case ③), spiral streamlines on the eddy boundary (Case ④), and the opposite extrema value (red spot) induced by multiple cores (Case ⑤) sometimes lead to resolving fake eddies because of the limitation of the detection method. Thus, the exceeding detection rate (EDR) is still inevitable in traditional detection methods. For instance, Yi et al., (2014) scrutinized that the EDRs of these methods in the South China Sea are around 70.3% for the OW method, 36.8% for the SLA-based method, and 14.2% for the HD method. As these methods detect eddies directly on single snapshots without further validation, fake eddies cannot be easily eliminated. The red spots are the fake eddy cores detected by these methods, which contribute to the EDRs.

All these methods are based on the direct detection of eddy snapshots in the horizontal plane without further validation in the temporal dimension, which limits the detection and tracking and causes exceeding detection. In this study, a novel eddy detection method was designed and developed to provide more accurate detection and tracking of eddies over an extended period, effectively improving the detection and tracking accuracy. The new detection method combines both the eddies' temporal and spatial features to detect eddies and then identifies the original eddies. Namely, it retrieves eddies from their temporal footprints on each section. The method developed in this study can avoid the aforementioned limitations (case ②, ③, ④, ⑤) as it detects eddies in both the temporal and spatial dimensions, which also allows the identification of weak and small-scale eddies. This study is organized as follows: Section 2 proposes the new detection scheme and the corresponding automated detection procedure, Section 3 implements the method to detect the Capricorn Eddies and decipher their general characteristics, discussions concerning both the method and Capricorn Eddies are presented in Section 4, and Section 5 provides a summary of this research.

2. Materials and methods

2.1. Schematics

Mesoscale eddies either migrate or locally wander, leaving their sectional paths in the temporal dimension (referred to as the SPTs in this study, Fig. 3). Namely, the temporal footprints of the eddies on sections will be recorded by the SPTs. Conversely, these paths (the SPTs) can also indicate the evolution of the original eddies over the corresponding sections. As bilateral conversions (eddies vs. SPTs) are not reproducible in time and space, the uniqueness of the SPTs is ensured for each eddy. Therefore, SPTs can be collected to identify the original eddies. This implies that the SPT method, even if the eddy appearance is missing for a few days, the SPT can still restore the original eddies over several sections. The overlapped SPTs cover the missing data after integration. Thus, the SPTs can be further analyzed and detected to identify the features of the original eddies, including their spatial scales, lifespans, and migrations.

An eddy leaves its specific SLA path over the section line from the time it first intersects the section until the time it leaves the section (upper plot in Fig. 3). This unique feature cannot be repeated in either time or space. The eddy path left on the section is called an SPT (the upper plot in Fig. 3) in this study. The principle of the SPT is shown in Fig. 3 as schematic plots of a propagating eddy. Once it passes a section, the eddy leaves its specific SPT in terms of this section (upper plot in Fig. 3). For example, it takes time t_1 to t_5 for the eddy to pass section x_0, thus its corresponding SPT over section x_0 covers from t_1 to t_5. Similarly, the SPTs left over each passed section are subsequently integrated, which will be further used to identify the original eddies.

Note that the SPT in Fig. 3 is regular ellipse because the given eddy is circular and evolve uniformly. In reality, eddies and SPTs are irregular in

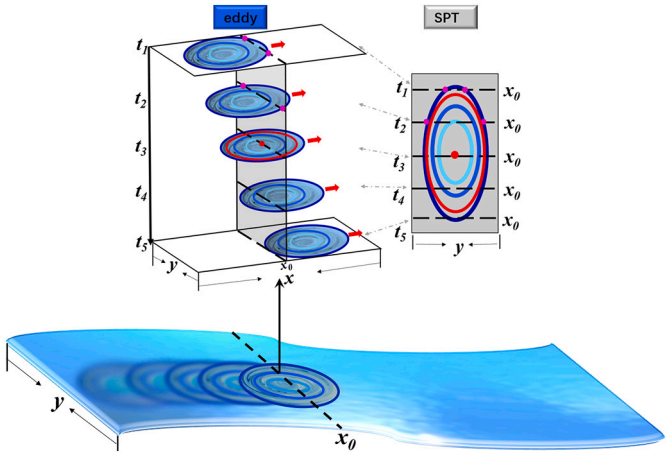

Fig. 3. Schematic plot of the conversion between the eddy and SPT. The horizontal bottom plot displays a propagating eddy along *x*-direction. The interconversion between the eddy and SPT on section x_0 is shown upper plot, in which the pink points are the intersection points at t_1 and t_2. The red point indicates the core of the eddy at t_3, when the eddy is at the strongest status. The red circle of the eddy can be used to determine the outermost of the SPT. (For interpretation of the references to colour in this figure legend, the reader is referred to the web version of this article.)

shape as eddies are vulnerable to the dynamic circumstances created by, for example, currents, neighboring eddies in the surrounding oceans, topography, and winds. Moreover, as most of the mesoscale eddies propagate zonally, eddy evolution paths over the meridional sections (i.e., south-north direction) are most suitable. Zonal sections can also be used, but require longer computing time and additional filtering procedures, as the eddies are most likely to ride on the zonally propagating planetary Rossby waves (Chelton et al., 2011).

The SPT schematic indicates the existence of an eddy in a horizontal plane, but is not conclusive, especially in a real ocean. The complicated circulation of the real ocean, such as the turbulence that is also revealed by the SLAs, might exist concurrently, and it is not very distinguishable from the SPT of eddies. Thus, the scientific questions were then revised to:

a) How can eddies be identified in an SPT map?
b) How can SPTs be better resolved with the appearance of eddies' motions on a similar scale?
c) What are the essential conditions for a more accurate detection of eddies?

The resolved SPT core (inner extrema) indicates the most mature status of the eddy during its evolution over this section. The SPT core (cx_3, cy_3, t_3) can be used to check the horizontal SLA map in the area ($cx_3 \pm x_r$, $cy_3 \pm y_r$) at t_3 and determine whether there is an eddy (closed contours encircle the SPT core). x_r and y_r are the pre-set radii used to determine the scope of the horizontal SLA map at t_3. As determined in a recent study (Chen and Han, 2019), the average radius of global eddies is approximately 70 km, and the maximum radius does not exceed 200 km. Therefore, to avoid underestimating the eddy's scale, x_r and y_r were set to 200 km as a default. If there is a closed contour encircling the SPT core (cx_3, cy_3) at t_3, the eddy's features at this time will be recorded. Otherwise, the closed contour does not correspond to an eddy, will be discarded. As the SPT is not a regular shape in most cases, the boundary of the SPT (SLA threshold) can be approximately determined by the eddy boundary (outermost SLA) at t_3. The temporal duration of the SPT indicates the lifespan of the eddy over the corresponding section. Note that there could be several SPT cores and corresponding thresholds within one SPT as the eddy may wander over a section and leave several discrete cores on one section. Thus, an integration of these processes is considered and included in the detection. As all the information regarding the cores, lifespans, and spatial scales over all the sections the eddy passes is achieved, the eddy characteristics and evolution can be determined.

2.2. Auto-SPT detection method

Based on the SPT framework, we developed an automatic eddy detection method. Fig. 4 shows the SPT detection procedure. Steps 1–7 depict the eddy detection processes in a representative section. Step 8 combines the processes for all the sections to identify the integrated eddies in the entire domain.

Step 1: Extract the two-dimensional (2D) SLA temporal variation over a geographic section ($lon = lon_1$, $lat_{(1\cdots i)}$, t) from the three-dimensional (3D) spatial and temporal SLA ($lon = lon_1$, lon_2, …, lon_i, $lat_{(1\cdots i)}$, t) data.

Step 2: Fetch the closed contours (lon_1, $lat_{(1\cdots i)}$, t) from the 2D time-series SLA map.

Step 3: Find the cores of the closed contours (lon_1, lat_1, t).

Step 4: Return to the horizontal SLA field ($lon_1 \pm \Delta lon$, $lat_1 \pm \Delta lat$, t_1) based on the gathered core information and examine if there is a corresponding eddy, where Δlon and Δlat are the radii of the horizontal field. As previously mentioned, the default values for the Δlon and Δlat are 200 km. If a closure SLA contour encloses the point (lon_1, lat_1), an eddy is identified. The diameter, intensity, and outermost SLA value of the eddy at t_0 can also be recorded.

Step 5: The outermost SLA value extracted from the horizontal SLA map returns to the closed SLA contours in Step 2. A corresponding SPT defined by the outermost SLA value is obtained.

Step 6: The temporal scale of the obtained SPT is regarded as the lifespan of the eddy over this section.

Step 7: The eddy found in Step 4 provides the diameter and intensity information.

Step 8: Based on the possible propagation speed, the detected features over different sections should have similar characteristics and temporal differences based on the calculation of the possible propagation speed induced by the planetary β effect. Furthermore, the resolved SPTs over neighboring sections have temporal and spatial overlaps. All the SPTs over the sections are then integrated to identify the original eddy and its evolution.

2.3. Method implementation in the study area

To further explain the scheme of the proposed SPT method, we applied the method in the SGBR region (Fig. 1) to detect the Capricorn Eddies. Fig. 5 shows the process from Steps 3 to 7 as an application of the SPT method over section S1 (153.8°E, Fig. 1) in 2009. In this study, we employed SLA data to conduct the detection. The SLA data were extracted from the Ssalto/Duacs gridded multi-mission altimeter, which is produced and distributed by the Copernicus Marine and Environment Monitoring Service (www.marine.copernicus.eu). The SLA data are based on a 20 year (1993–2012) mean with a 0.25° × 0.25° horizontal resolution and daily temporal resolution from 1993 to 2018. Fig. 5a shows all the closed time-series SLAs (primary SPTs), and Fig. 5b indicates the potential cores (irregular closures) of the corresponding SPT contours in Fig. 5a. As we found the time and location of the core, we could track it back to a horizontal plane to determine if there is an eddy. Fig. 5d is an example of a non-eddy case, whereas Fig. 5c and e show the case of a cyclonic eddy and an anti-cyclonic eddy. As shown in Fig. 5a and b, not all the primary SPT contours correspond to eddies. Thus, the self-validation procedure (Steps 4–5) must be activated in the detection method in order to efficiently avoid exceeding detection.

Following the above detection steps in Section 2.2, we present a case of SPT detection in S1 (red dashed line in Fig. 1). As shown on the right of Fig. 6, an eddy was locally generated on Day 65 and continued growing until Day 80. Then, it began decaying and finally dissipated on

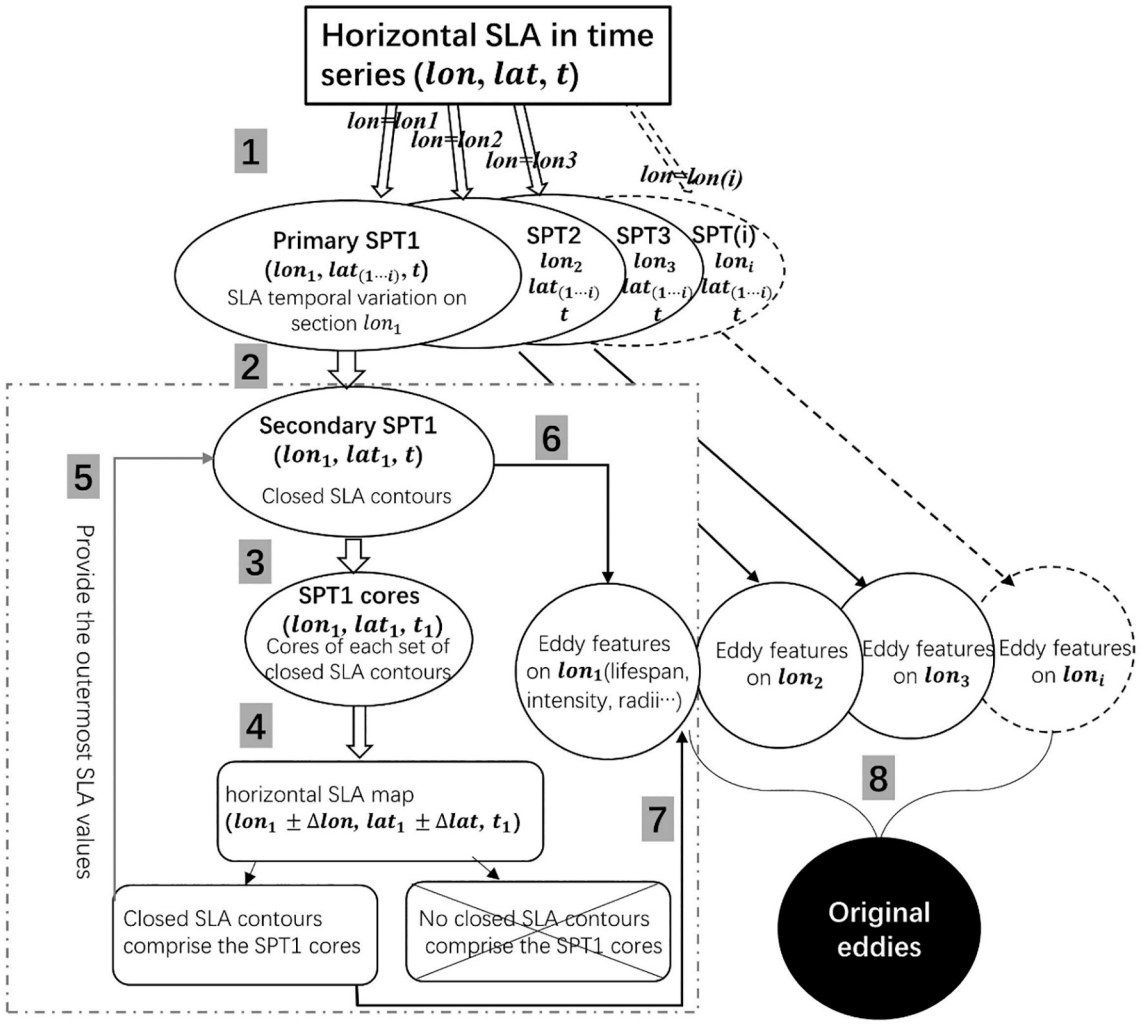

Fig. 4. Block diagram of the SPT method showing the detection processes.

Day 105. During its evolution, it overlaid section S1. From the corresponding temporal SLA variations in S1 (left part in Fig. 6), we observe an ellipse contour. The ellipse contour occurred on Day 65 and extended to the largest scope on Day 80 before decreasing. In terms of time, the evolution of the ellipse was consistent with the eddy evolution. In space, the eddy occupied the S1 between 22°S and 25°S, which also overlaid the scope of the contour. Thus, the detailed evolution of the eddy in S1 can be captured well by the SPT. When the eddy evolves over S1, from the first time it interacts with S1 till it leaves S1, the SPT stores all the possible information including the lifespan, the radius, the intensity and the evolution processes.

3. Results and discussion

The current understanding of Capricorn Eddies is derived from limited observations in several individual years and associated assumptions of their possible characteristics on local circulation. Using the newly developed detection method, we audited the Capricorn Eddies. In this section, the validation of the new method is firstly presented. We then summarized the numbers, types, spatial and temporal scales, and intensity of the Capricorn Eddies. Seasonal variations were explored to evaluate the possible intra-annual factors. Corresponding possible mechanisms for the above features of the Capricorn Eddies are also explored.

3.1. SPT method validation

The SPT method contains a self-validation procedure (Steps 4–5) that eliminates fake eddy features and ensures the accuracy of the detection rate. In this section, additional validations by other observations are adopted to provide lateral evidence. Specifically, we examined Argo, mooring, and previous study data to further validate our detection results. Furthermore, we also compare the SPT method with the traditional method by exploring some cases.

3.1.1. Validated by the observations

There are several observations for supporting the existences of the Capricorn Eddies. For example, an Argo profiler (#5903639) passed through the study area, capturing the occurrence of a Capricorn Eddy by providing temporal temperature profiles of the region. A previous study by Mao and Luick (2014) also revealed several Capricorn Eddies. The mooring data from the site GBROTE provided by the Australian Institute of Marine Science (Fig. 1) were previously used to examine Capricorn Eddies (Choukroun, 2010). When a Capricorn Eddy occurs and its edge is close to the GBROTE, a northwest velocity from the GBROTE can be an indicator for Capricorn Eddies, but it is not conclusive as coastal trapped waves along the slope also trigger periodic northwest flows. All these findings were used to validate our results. Fig. 7 shows all the detected Capricorn Eddies from 1993 to 2018 and lateral validations from Argo (green band), previous studies by Mao and Luick (2014, pink bands), and the mooring data (blue horizontal lines with black arrows).

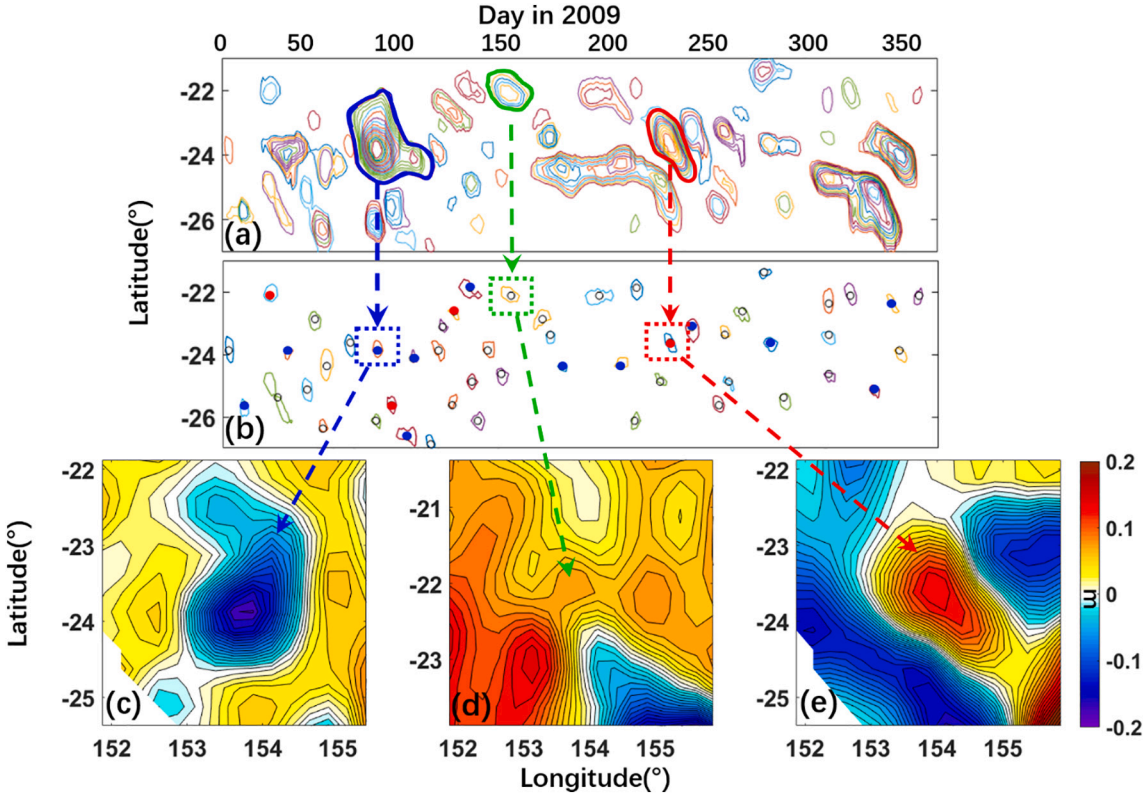

Fig. 5. A case study of S1 in 2009 showing the main process of the SPT. All the enclosed contours in (a) are the potential SPT. The enclosed SPTs in red and blue in (a) are potential eddy SPTs selected as two cases to illustrate the self-validation processes. Corresponding SPT cores are shown in (b) where red cores for anti-cyclonic eddy and blue for cyclonic eddy. The black rings in (b) are the fake cores of the SPTs which don't represent eddies. (c), (d), (e) show the corresponding horizontal sea level anomaly (SLA) features based on the information of these three cases provided in (a) and (b). (For interpretation of the references to colour in this figure legend, the reader is referred to the web version of this article.)

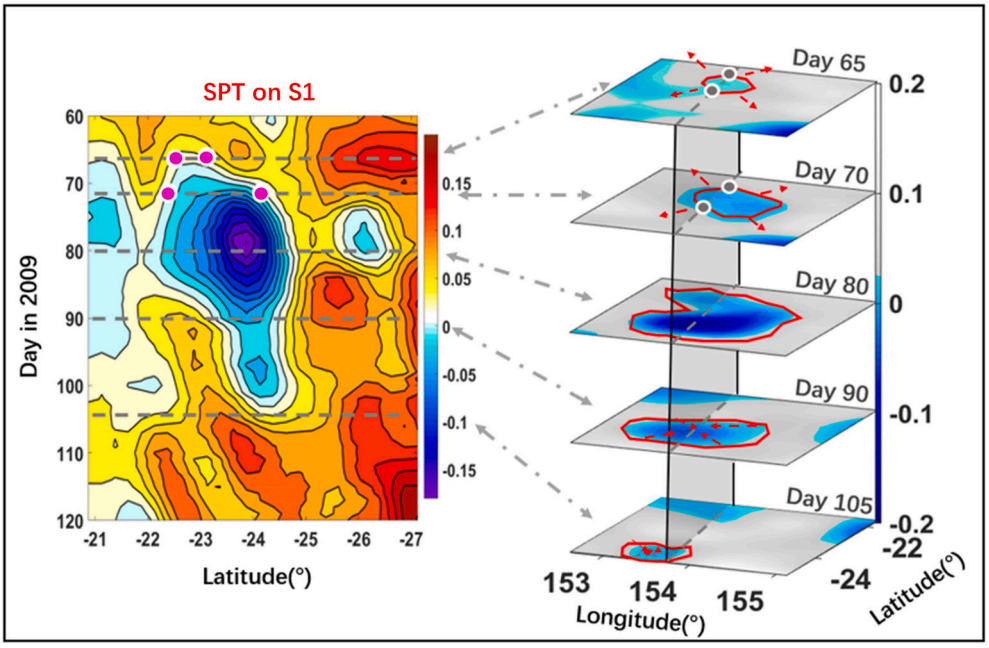

Fig. 6. A typical case of the conversation between a Capricorn Eddy (right) and its corresponding SPT (left) in 2009.

Fig. 7b, c, and d elaborate the details of the validation for the Capricorn Eddies detection. As previously mentioned, the presence of the Capricorn Eddies is at first revealed by northeastward flow at the mouth of the Capricorn Channel (Woodhead, 1970; Griffin et al., 1987). The velocity directions recorded by the mooring site GBROTE (Fig. 1) were extracted and analyzed to further validate the schematics in Section 2.2 (arrows in Fig. 7a and b). It should be noted that the mooring validation can be only used for detected eddies, but cannot be directly

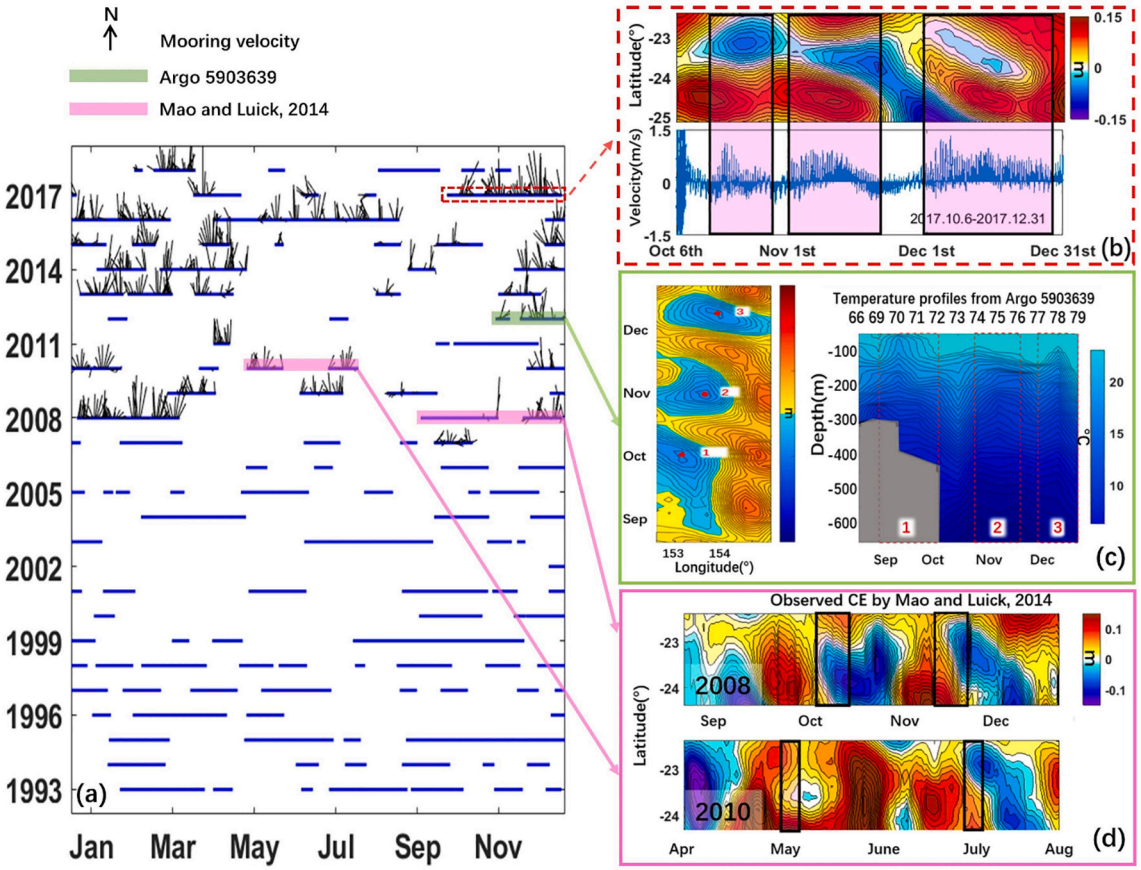

Fig. 7. (a) SPT detected Capricorn Eddies (blue lines) from 1993 to 2018. Black arrows on the blue lines are the components of u and v velocity vectors from the mooring GBROTE. Red dashed band comprises a case study period for (b). Green band indicates the validation by Argo 5,903,639. Pink bands are the detected Capricorn Eddies by Mao and Luick (2014). (b) A case study of the GBROTE mooring, which validates the detected Capricorn Eddies in 2017. The upper plot is the SPT on section 153.5°E. The lower plot is the finer velocity vectors. The velocities are also the components of the u and v velocities. (c) Temperature data (right panel) from Argo 5,903,639 that validates the Capricorn Eddies detected in 2016. Left Fig.panel is the corresponding SPT on section −23.5°. (d) Eddy occurrences reported by Mao and Luick (2014) (black boxes) in 2008 and 2010, and the corresponding SPTs (colorful contours). (For interpretation of the references to colour in this figure legend, the reader is referred to the web version of this article.)

used as a signal of eddies as the northward flow with a period of 8–14 days could also be triggered by coastal trapped waves (Griffin and Middleton, 1986; Liao and Wang, 2018). Moreover, not every Capricorn Eddy is close enough to the GBROTE to cause a northward flow. Based on the Argo temperature profiles, remarkable isothermal uplifting can be observed at the time when the Capricorn Eddy signals occur in the SPT map (Fig. 7c). The Argo only provides single profiles to manifest the eddy signals. Meanwhile, the SPT could provide the entire evolution details of each eddy. Mao and Luick (2014) reported several eddy events in 2008 and 2010 (black squares in Fig. 7d) that were detected using SPT methods. Here, the SPT detected much longer lifespans for these eddies than their previously reported lifespans. For example, Mao and Luick (2014) found that the detected Capricorn Eddies in October 2008 lasted for 10 d, whereas the lifespan indicated by a single SPT was over 1 month. This discrepancy in lifespan suggests that there is a need for an accurate detection method for detecting weak and transient eddies.

3.1.2. *Comparison with the SLA-based method by case studies*

As demonstrated in Section 1, traditional detection methods may not be feasible to detect eddies with inconspicuous surface appearances or detect fake eddies by mistake. Specifically, for the Capricorn Eddies, which are transient phenomena with weak intensity, traditional detection methods cannot be suitably applied. As the SLA-based method has been widely adopted for eddy detection, we invoked some results from the SLA-based method to illustrate discrepancies. Fig. 8 shows a series of SLA-based detection data in the study region from Day 108 to Day 127 and from Day 218 to Day 219 in 1993 (Tian et al., 2020; http://coadc.ouc.edu.cn/tfl/) as examples. During this period, three anti-cyclonic eddies (AEs) and four cyclonic eddies (CEs) generated in the study region were detected and tracked using the SLA-based method. Eddies with consecutive and intensified surface features (e.g., AE1 and AE2) can be successfully detected and tracked, demonstrating the efficiency of the traditional detection method. However, some exceptions were observed, as shown in Fig. 8. The aforementioned Case ② (Fig. 2b) has already contended that the traditional eddy tracking procedure may miss some eddies if the surface feature changes abruptly in the next snapshot. For example, CE1 and CE2 should be classified as the same eddy as its evolution from Day 108 to Day 110 can be consecutively observed. Moreover, CE2 is not dissipated after Day 112, but has not been detected by the SLA-based method. As we show in Case ③ (Fig. 2c), the traditional method may miss eddies with irregular shapes. By contrast, the SPT method is able to solve above problems. A consistent CE is observed from Day 105 to 120 in 1993 from the SPT detection. Fig. 7a shows the consistent detection and tracking of this eddy using the SPT in 1993. Furthermore, the detection of AE3 is an example of a misleading detection, such as in Case ④ (Fig. 2d). CE4 is a fake eddy between two anti-cyclonic eddies as we declared in Case ⑤. As is shown in Fig. 7a, this fake eddy is not captured by the SPT method. These detection problems can be attributed to the irregular shape of the mesoscale eddies during their evolution. Therefore, traditional detection methods based on snapshots may not precisely resolve the eddies in the study region, wherein the local eddies have small temporospatial scales.

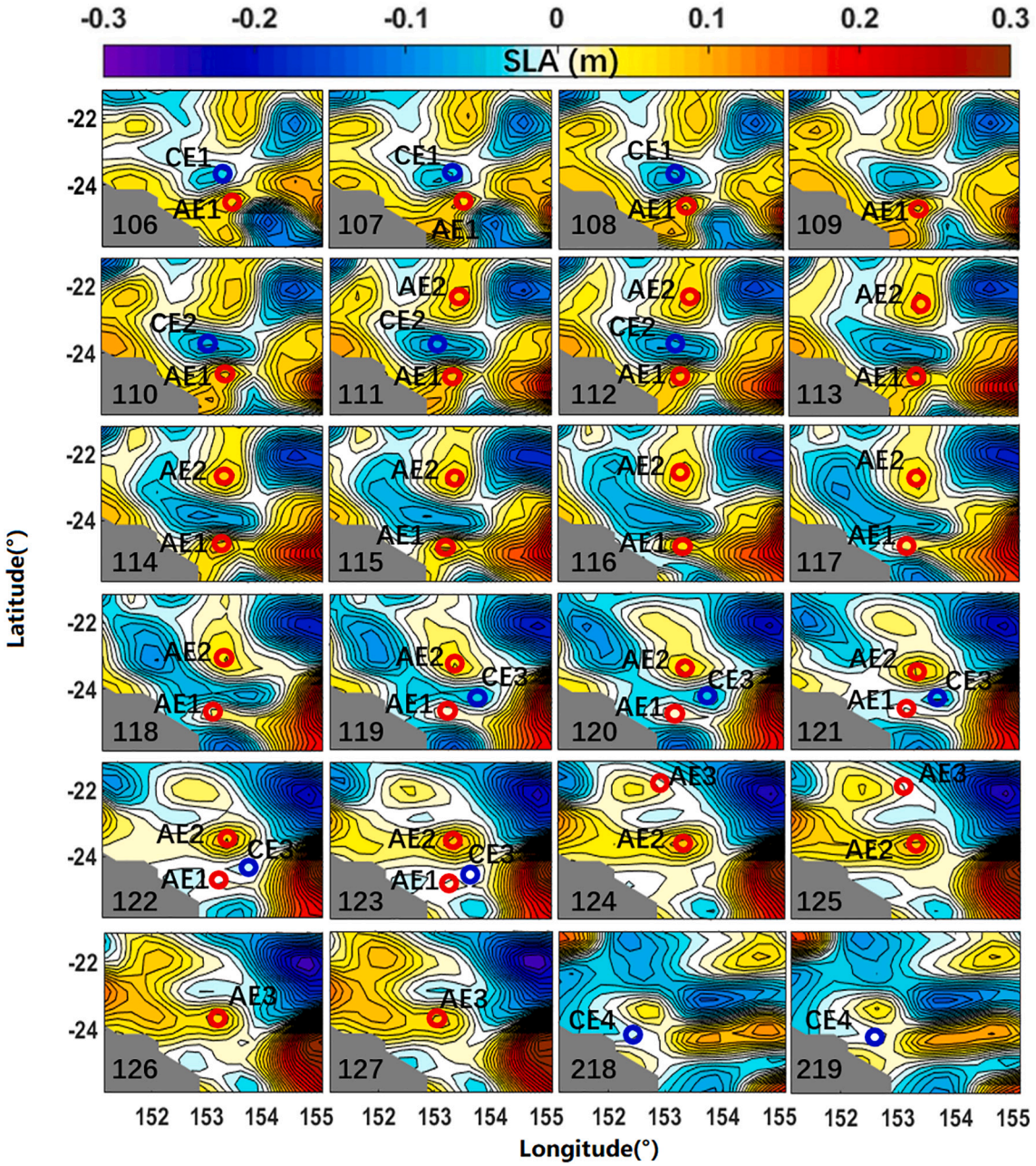

Fig. 8. Eddies detected in the study region using the sea level anomaly (SLA)-based method from Day 108 to Day 127 and from Day 218 to Day 219 in 1993 (The Day is denoted at the lower left corner of each panel. Detection data source is from http://coadc.ouc.edu.cn/tfl/). Red circles indicate the resolved core of anti-cyclonic eddies (AEs), while the blue circles indicate those of the cyclonic eddies (CEs). (For interpretation of the references to colour in this figure legend, the reader is referred to the web version of this article.)

The developed SPT method was designed based on the temporal paths over sections rather than a single eddy snapshot. Each detected SPT stores the information of an eddy's evolution over a section for several days (varying based on the eddy's scale and location, usually longer than 1 week). The SPT also comprises evolution information from the neighboring sections. Each SPT can be validated by tracking back to the original eddy feature to check whether it is real or fake. These procedures increase the accuracy of detection. The method developed in this study detected weak and small-scale Capricorn Eddies (e.g., CE1 and CE2 were consistently detected as one by the SPT; Fig. 7a). Thus, this method could be further implemented in other regions to check the unrevealed eddies that were missed by the traditional method.

3.2. Census of Capricorn Eddies

In this section, a long-term detection of the Capricorn Eddies will provide us an integrated understanding of the Capricorn Eddies, which fill the gaps in previous studies. The basic statistical features and their behind mechanisms will be explored in detail.

3.2.1. Statistical features of the Capricorn Eddies

We conducted a detection of Capricorn Eddies over 26 years from 1993 to 2018 as a census. Fig. 9 shows the details of all the detected eddies in the study area, including their lifespans, spatial scales, and amplitude distributions. As shown in Fig. 9, the majority of the eddies' lifespans range from 10 d to 40 d, the radii range from 50 km to 150 km,

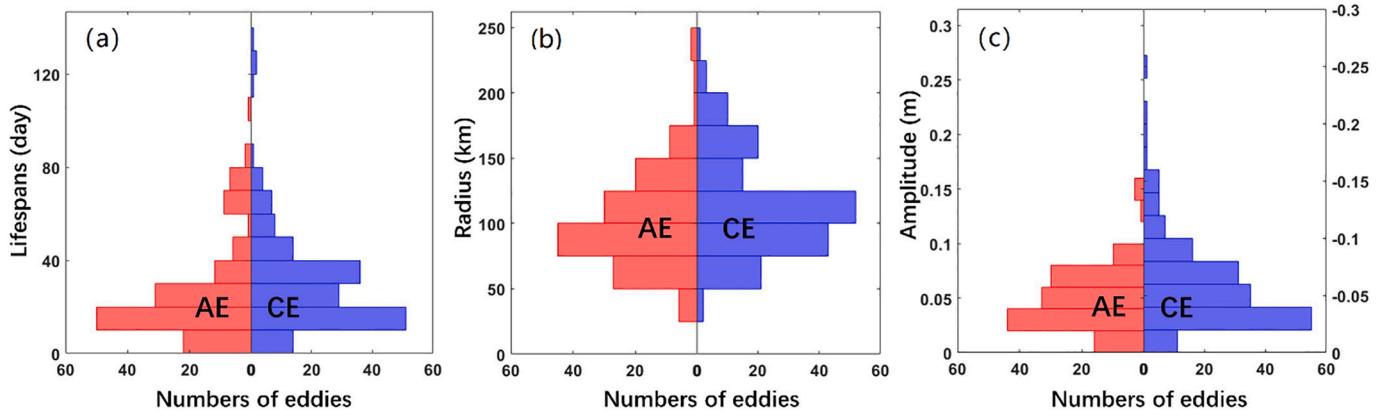

Fig. 9. Histograms of the eddies' lifespans (a), radii (b), and amplitudes (c). Blue bars indicate the cyclonic eddies (CEs, namely the Capricorn Eddies), and red bars represent the anticyclonic eddies (AEs). (For interpretation of the references to colour in this figure legend, the reader is referred to the web version of this article.)

and the amplitudes range from 2 cm to 8 cm. Limited by the resolution of the SLA data, eddies with lifespans shorter than 10 d and amplitudes less than 2 cm (Dufau et al., 2016) are regarded as unreliable results, and are thus eliminated in the following analysis. As there are many eddies with short lifespans, small radii, and amplitudes, these results confirm that the Capricorn Eddies are transient and intermittent. The proportions of anti-cyclonic eddies (AEs) and cyclonic eddies (CEs, the Capricorn Eddies) are approximately equal to those in the global oceans (Chelton et al., 2011). Previous studies focusing on CEs concluded that they were generated by the EAC without mentioning AEs. However, our detection indicates that the local ocean favors generating both AEs and CEs, although the generation mechanisms require further exploration that is not within the scope of this study. The targeted Capricorn Eddies are particularly the cyclonic eddies, only the CEs will be explored in the later analysis.

The SPT detection updated our current understanding of Capricorn Eddies. Specifically, their occurrences (approximately 6/year) are higher than that found previously (approximately 2/year, Mao and Luick, 2014). Their characteristics, including their lifespans, radii, intensities, and temporal evolutions, were also yielded. The Capricorn Eddies detected by the SPT method had lifespans ranging from 10 d to 140 d, in which the majority are between 20 d and 40 d. Choukroun (2010) observed a high-energy burst between 20 d and 40 d from the wavelet power spectrum of the local velocity at GBROTE, confirming the Capricorn Eddies are pronounced in the local circulation. The location of the Capricorn Eddies may be a factor that constrains their lifespans. As the Capricorn Eddies are generated in the lee of the SGBR, they eventually reach the coast, where they diminish. The radii of the Capricorn Eddies range from 50 km to 150 km as the eddies are mostly generated by the EAC. Thus, their locations are constrained between 152°E and 155°E (Fig. 1). Some exceptions with large radii of over 150 km are the westward-propagating eddies from the east of the study area. However, the proportion of these eddies is only 27% of the total number of detected eddies, indicating that most of the Capricorn Eddies are locally generated. The amplitudes of the Capricorn Eddies were generally between 2 cm and 8 cm. It is also worth noticing that for the global ocean long-lived eddies, only 60% have amplitudes of approximately 5 cm (Chelton et al., 2011), and although Capricorn Eddies were defined as small-scale and weak hydrographic features, 50% of them had amplitudes larger than 5 cm.

Capricorn Eddies have favorable scales (radii between 50 km and 150 km), lifespans (between 10 d and 40 d), and amplitudes (between 2 cm and 8 cm), as shown in Fig. 9 and Fig. 10. These scales are possibly controlled by regional circulation, such as the EAC and outflow from the Capricorn Channel. However, the relationship between these characteristics of Capricorn Eddies remains unclear. It was suggested that longer-lived eddies usually have larger amplitudes, radii, and vorticities

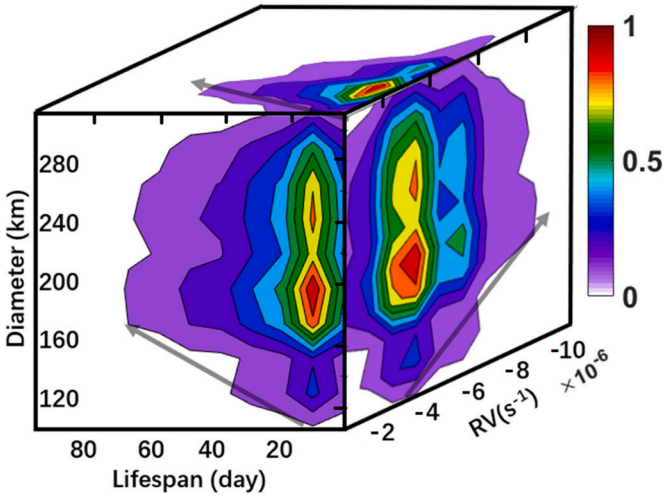

Fig. 10. Three-dimensional histograms of the lifespan, diameter, and relative vorticity of cyclonic eddies (CEs). Colorbar denotes the unified distribution of these characteristics.

(Chelton et al., 2011). A similar finding was observed in this study. In this section, we explore some Capricorn Eddy characteristics and their possible internal connections. Most CEs have lifespans shorter than 20 d, with diameters ranging from 120 km to 250 km. Their relative vorticity centralizes between -2×10^{-6} s^{-1} and -4 $\times$ 10^{-6} s^{-1}. The longer-lived Capricorn Eddies have a larger spatial scale and stronger intensity (Fig. 10), whereas the shorter-lived Capricorn Eddies can have both large/small scales and strong/weak intensities. A similar result was found by Chen and Han (2019). Moreover, as demonstrated in Type III eddies, which have a longer lifespan, and can receive energy injection for a short time and then diminish with small vorticities. Their intensities are not directly linked to lifespan. It is possible that this phenomenon is universal in the oceans, but requires further exploration and explanation.

3.3. Evolution of Capricorn Eddies

In previous studies, the factors affecting the evolution of eddies have been explored using case studies and were identified as the EAC and outflow from the Capricorn Channel (Mao and Luick, 2014). However, the statistical evolution processes have not been studied, and the detailed evolution process during the lifespan of Capricorn Eddies remains unknown. The wide range of characteristics, including lifespans, radii, and intensity, may be related to the evolution process.

Table 1
A census of the Capricorn Eddies detected using the SPT method. The Capricorn Eddies are classified into three types based on their different evolution types.

1993–2018	Total	Type I	Type II	Type III
Numbers of eddies	147	48	60	39
Rossby number	0.05	0.067	0.056	0.044
Average lifespan (day)	26	18	27	30
Average diameter (km)	180	170	180	190

Table 1 summarizes the characteristics of the Capricorn Eddies observed over the study period. In total, there were 147 Capricorn Eddies, with an averaged Rossby number of 0.05, an averaged lifespan of 26 days, and an averaged radius of 90 km. To understand the details of the Capricorn Eddies, we divided them into three types based on their evolutions of intensity, which have two stages, growing and decaying. The period before the occurrence of the largest intensity (relative vorticity) is defined as the growing stage, whereas after that is the decaying stage. Type I denotes an eddy in which the duration of the growing period roughly equals the decaying period. Type II denotes an eddy in which the growing period is longer than the decaying period. If the eddy is not Type I or II, it is classified as Type III. As summarized in Table 1, we can see that Types II and III are more stable with longer lifespans.

Capricorn Eddies could generate and disappear in equal periods as Type I. However, the total lifespan, growing stage, and decaying stage of this type are shorter than those of the other two types as is shown in Fig. 11. Thus, the majority of this type has lifespans shorter than 20 d, these eddies are possibly stimulated to generate and grow in a shorter time with less energy input and then decay quickly. The corresponding radii are also smaller than those of the other two types. In contrast, Type II eddies continue growing over a longer period, but decay in a shorter time. As Type II eddies have a longer growing period, they are prone to form larger spatial scales. Finally, Type III eddies grow quickly to form an intensified eddy with a smaller radius, and then decay with the expansion of their radii. As previously mentioned, more intensified eddies usually perform more coherently with smaller radii and longer lifespans. Further, it seems that Type III eddies receive much of their energy in a short period at the beginning of their life, while Type II eddies continue receiving energy during most of their life. In general, the largest spatial scales are consistent with the strongest intensities. The consistent proportions of Types I, II, and III, are 70%, 70%, and 50%, respectively (Fig. 11). As the evolution of the Capricorn Eddies is attributed to the EAC and outflow from the Capricorn Channel, these types can be further explained by their temporal distribution and EAC variation.

The generation of the Capricorn Eddies is mainly related to the variation of the EAC including their strengthens and locations as mentioned in the Introduction. Because of a lack of observational data and the poor quality of the SST images in the summer (cloud effects), the suspected Capricorn Eddies were only observed in September or October in 1987, 1988, and 2008 (Burrage et al., 1996; Kleypas and Burrage, 1994; Weeks et al., 2010). Later, Mao and Luick (2014) speculated that Capricorn Eddies exist at other months of the year, based on two years' observations. However, owing to the limitation of observation, they could only provide a hypothesis without a definitive conclusion. Thus, the understanding of Capricorn Eddy occurrences is not comprehensively understood. Do Capricorn Eddies occur in other months of the year? Do different eddy types have distinguished temporal variability? In this section, we explore monthly Capricorn Eddy activities in order to answer these questions.

As shown in Fig. 12, Capricorn Eddies can occur throughout the year. However, there are some disparities in different months, in which the numbers range from 8 to 18. In general, more eddies are generated in the

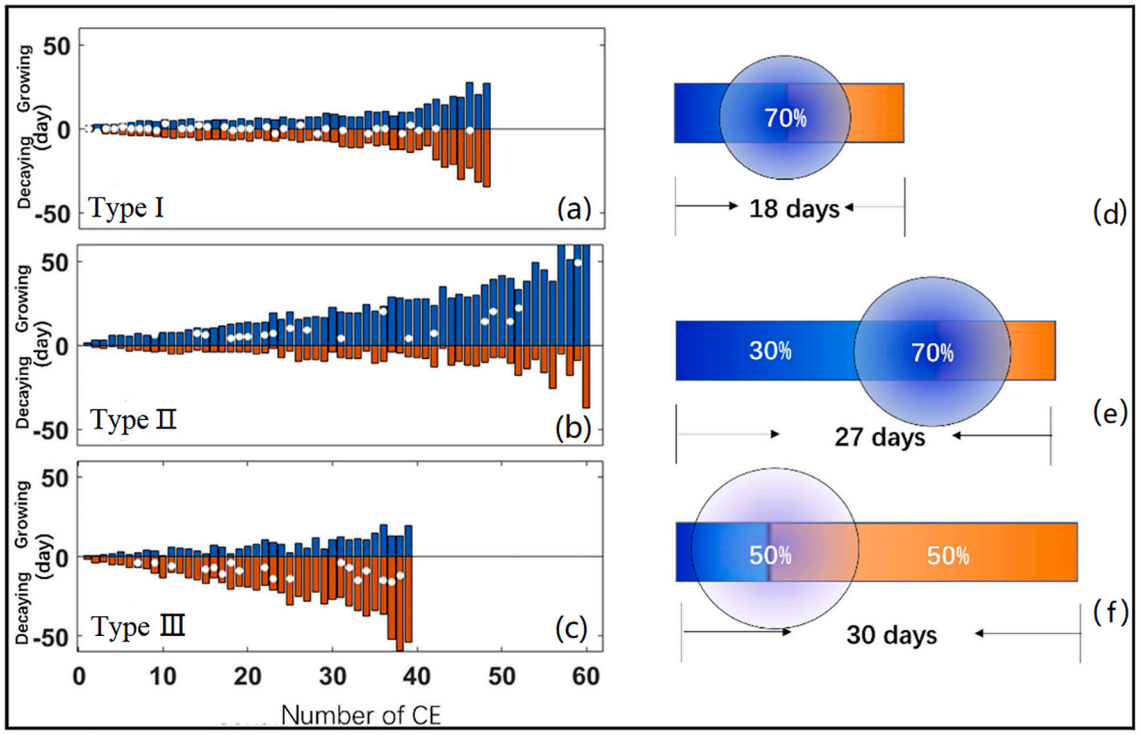

Fig. 11. Three types of Capricorn Eddies. (a): eddy in which the growing period roughly equals the decaying period (Type I); (b): eddy growing period is much longer than the decaying period (Type II); (c): eddy growing period is much shorter than the decaying period (Type III). Blue bars indicate the growing period, and the red bars the decaying period. The locations of the white spots are the typical time when the largest scales occur. (d), (e), (f) are the corresponding statistics of the evolution for Type I, II, III. The circle size in the indicates the corresponding radii, while the fill shows the rough intensity. The percentages show the proportions of eddies in which the largest radii and largest intensities occur simultaneously. (For interpretation of the references to colour in this figure legend, the reader is referred to the web version of this article.)

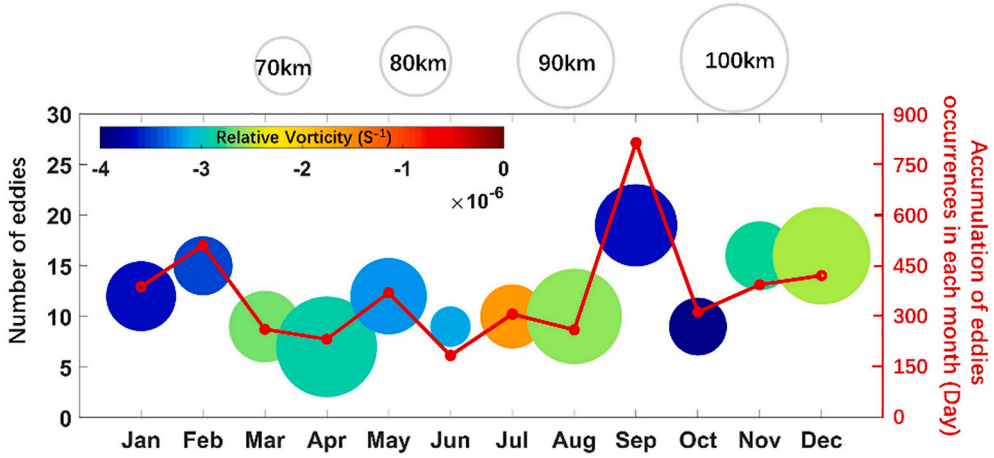

Fig. 12. Monthly variation of the Capricorn Eddy occurrences. Red line indicates the trends of the monthly total eddy occurrence days over the study period. Circles depict the monthly-averaged radii. Colors in the circles indicate the monthly averaged relative vorticities of the Capricorn Eddies. (For interpretation of the references to colour in this figure legend, the reader is referred to the web version of this article.)

austral summer (December–February) and less in the winter. Some discrepancies occur in September and October. The total number of occurrence days in each month exhibited a similar pattern. Further, the eddies in summer usually have higher intensities, when previous studies mainly observed Capricorn Eddies, while the eddies in winter have lower intensities. These features can be elucidated by EAC variability. Specifically, the EAC flow is the strongest in the austral summer, as reported by Ridgway and Godfrey (1997), enabling it to inject more energy into the eddy field to stimulate eddy generation. Latterly, Xie et al., (2021) also reported that the EAC tends to be closer to the coast in austral summer than that in winter, which may favor the generation of the Capricorn Eddies. However, the monthly radii of the Capricorn Eddies do not present an analogous trend. As reported by Chen and Han (2019), most eddy features, including the amplitude, vorticity, and kinetic energy, are related to the lifespan. However, the radii of the eddies, especially those long-lived ones, are usually isolated to the lifespan (Chelton et al., 2011). Thus, the monthly radius distributions of the Capricorn Eddies do not exhibit a significant seasonality.

Most of the Capricorn Eddies' characteristics present distinct seasonal variation, as aforementioned, which can be roughly explained by the EAC variation. Specifically, the evolution of eddies determines their features. Thus, we explored the possible mechanisms for understanding the temporal variation in the evolution of eddies. Fig. 13 shows the monthly distributions of the three types of Capricorn Eddies. In general, Type I eddy is more prevalent in austral winter (June–August), while Type II and III eddies occur more frequently in austral summer (December–February), with some discrepancies.

As reported in previous studies (Andrews and Furnas, 1986; Brinkman et al., 2001; Xie et al., 2021), the EAC tends to be the strongest and occasionally intrudes the shelf through the reef in October. The adjacent

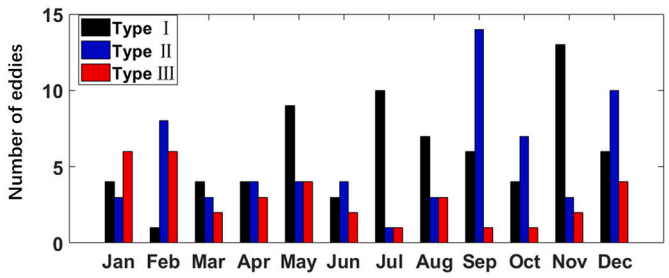

Fig. 13. The monthly occurrences of the three Capricorn Eddy types over 26 years.

of the EAC to the central GBR is the strongest in September and October (Andrews and Furnas, 1986; Church, 1987; Brinkman et al., 2001). Moreover, Mao and Luick (2014) found that the generation of Capricorn Eddies is attributed to the increasing strength of the EAC. The majority of the eddies generated in September and October are Type II eddies, which receive continuous extensive energy during their lifespans. However, as Type II eddies grow quickly, they push the EAC away from the shelf, cutting off the energy source as mentioned by Mao and Luick (2014). Thus, the Type II eddies diminish in a short time. Conversely, Type III eddies occur more frequently in January and February, which is when the EAC is stronger than that in winter but weaker than that in September and October, enabling it to persistently provide energy to the eddies. In this case, Type III eddies can survive longer with less energy injection at the beginning of their lives. In contrast, the occurrences of short-lived Type I eddies fluctuate more throughout the year. In particular, they appear more frequently in May, July, and November, during which they exhibit weaker intensities. Thus, the Type II and III eddies usually occur when the EAC is stronger, while Type I eddies may survive when local circulation is not strong. These results are a primary hypothesis for Capricorn Eddy generation mechanisms and deserves further exploration to scrutinize their behavior in different months.

4. Conclusions

In this study, a novel eddy identification method was developed to identify Capricorn Eddies using SLA data from 1993 to 2018. Unlike the existing eddy detection methods that detect eddy snapshots directly in the spatial dimension, the SPT method fully recognizes the spatiotemporal coverage of the SLAs to identify the mesoscale eddies. An eddy's SPT represents some features of the eddy during its period over a section. All the features left over all the sections it passes or stays reconstitute the original eddy. The SPT method improves the accuracy of the detection, as it is guaranteed by the time-series footprint of the eddies and contains self-validation processes. This method also strengthens the tracking procedure by using overlapped SPTs, in which SPTs over neighboring sections overlap as they contain similar time-series, validating and covering each other under any condition. Thus, eddies with short lifespans and intermittent surface features can also be well identified.

The presence of Capricorn Eddies is profound on the local scale. Thus, local projections and a comprehensive understanding of possible changes are critical for effective natural ecosystem management. As Capricorn Eddies feed the upwelling system and greatly affect the local ecosystem, there is a significant value in understanding the Capricorn Eddies. However, previous studies on Capricorn Eddies did not provide a

comprehensive picture of their characteristics, including their quantity, lifespans, intensity, temporal and spatial scales, and seasonal variations, because of limited observations. It is also difficult for traditional eddy-detection methods to address the detection of eddies with temporal inconspicuous features or short-lived eddies, such as Capricorn Eddies. As Capricorn Eddies are defined as transient and intermittent phenomena, a more precise detection method is required.

This novel approach provides an identification method for Capricorn Eddies and has been validated by several observations. Furthermore, the occurrences and lifespans of the Capricorn Eddies during the period of 26 years were also obtained, enabling us to determine the frequencies and general characteristics of the Capricorn Eddies, as well as their possible relations. For example, short-lived eddies can tolerate both large/small spatial scales and high/low intensities, whereas long-lived eddies usually have larger spatial scales and higher intensities. Meanwhile, medium-lived eddies have a smaller intensity than either short-lived or long-lived eddies do. This unidirectional behavior might be a universal phenomenon, but requires further verification and explanation.

This study also found that Capricorn Eddies, in general, vary seasonally. Specifically, they more frequently appear in the austral summer and less in the winter, with some exceptions in September and October. This seasonal variation can be attributed to the seasonality of EAC, and the exceptions are possibly attributed to the adjacent of the EAC to the Great Barrier Reef in its formation stage. Further, this study provides the statistics of eddy characteristics based on surface features. To explore the impact on the ecosystem, an understanding of local multidimensional dynamics should be further explored.

As found by Amores et al. (2018), only 10% of the total global eddies can be captured owing to the current SLA resolution and detection methods. Chen and Han (2019) further declared that over 60% of global eddies are overlooked if only eddies with lifespans longer than four weeks are counted. The developed SPT method in this study provides a more accurate pathway for inspecting these unrevealed eddies. For instance, the method could be implemented in the 'eddy desert' region (Chelton et al., 2007) to check if transient eddies exist. Furthermore, the SPT method can avoid breaking one eddy lifespan into several ones by consistently realizing the eddy footprint, which may provide a new census of global eddies' number and life.

This study does not attempt to present the possible merging and splitting processes as they are not defined as frequent processes in this region and thus do not dramatically affect the current conclusion. The multiple core eddies are considered as individual eddies as the definition of the multiple core is nebulous. These will be included in future work to understand the possible interactions in a finer scheme. More detailed dynamic processes of the eddy interaction are possibly achieved in the future.

CRediT authorship contribution statement

Li Zhibing: Conceptualization, Methodology, Data curation, Writing – original draft, Formal analysis, Visualization. **Cai Zhongya:** Investigation. **Liu Zhiqiang:** Conceptualization, Methodology, Supervision, Writing – review & editing. **Wang Xiaohua:** Writing – review & editing. **Hu Jianyu:** Writing – review & editing.

Declaration of Competing Interest

The authors declare that they have no known competing financial interests or personal relationships that could have appeared to influence the work reported in this paper.

Acknowledgments

This work was supported by the National Natural Science Foundation of China (41776027, 41906016, 91958203), the Key Special Project for Introduced Talents Team of Southern Marine Science and Engineering Guangdong Laboratory (Guangzhou) (GML2019ZD0210), and the Science and Technology Development Fund, Macau SAR (SKL-IOTSC(UM)-2021-2023, SRG2020-00022-IOTSC). This is publication number 86 of the Sino-Australian Research Centre for Coastal Management.

References

Amores, A., Jordà, G., Arsouze, T., Le Sommer, J., 2018. Up to what extent can we characterize ocean eddies using present-day gridded altimetric products? J. Geophys. Res. Ocean 123 (10), 7220–7236. https://doi.org/10.1029/2018JC014140.

Andrews, J.C., Furnas, M.J., 1986. Subsurface intrusions of Coral Sea Water into the central Great Barrier Reef: I: structures and shelfscale dynamics. Cont. Shelf Res. 6, 491–514. https://doi.org/10.1016/0278-4343(86)90020-8.

Bailleul, F., Cotté, C., Guinet, C., 2010. Mesoscale eddies as foraging area of a deep-diving predator, the southern elephant seal. Mar. Ecol. Prog. Ser. 408, 251–264. https://doi.org/10.3354/meps08560.

Brinkman, R., Wolanski, E., Deleersnijder, E., McAllister, F., Skirving, W., 2001. Oceanic inflow from the Coral Sea into the Great Barrier Reef. Estuar. Coast. Shelf Sci. 54, 655–668. https://doi.org/10.1006/ecss.2001.0850.

Burrage, D.M., Steinberg, C.R., Skirving, W.J., Kleypas, J.A., 1996. Mesoscale circulation features of the Great Barrier Reef region inferred from NOAA satellite imagery. Remote Sens. Environ. 56 (1), 21–41. https://doi.org/10.1016/0034-4257(95)00226-X.

Chaigneau, A., Pizarro, O., 2005. Eddy characteristics in the eastern South Pacific. J. Geophys. Res. Ocean 110 (C6). https://doi.org/10.1029/2004JC002815.

Chelton, D.B., Schlax, M.G., Samelson, R.M., de Szoeke, R.A., 2007. Global observations of large oceanic eddies. Geophys. Res. Lett. 34, L15606. https://doi.org/10.1029/2007GL030812.

Chelton, D.B., Schlax, M.G., Samelson, R.M., 2011. Global observations of nonlinear mesoscale eddies. Prog. Oceanogr. 91 (2), 167–216. https://doi.org/10.1016/j.pocean.2011.01.002.

Chen, G., Han, G., 2019. Contrasting short-lived with long-lived mesoscale eddies in the global ocean. J. Geophys. Res. Ocean 124 (5), 3149–3167. https://doi.org/10.1029/2019JC014983.

Choukroun, S., 2010. School of Engineering Physical Sciences. In: The Surface Circulation of the Coral Sea and Great Barrier Reef. http://eprints.jcu.edu.au/24024.

Church, J.A., 1987. East australian current adjacent to the great barrier reef. Aust. J. Mar. Freshwater Res. 38, 671–683. https://doi.org/10.1071/MF9870671.

Cotté, C., Park, Y.H., Guinet, C., Bost, C.A., 2007. Movements of foraging king penguins through marine mesoscale eddies. Proc. R. Soc. B 2742385–2742391. https://doi.org/10.1098/rspb.2007.0775.

Dragon, A.C., Monestiez, P., Bar-Hen, A., Guinet, C., 2010. Linking foraging behaviour to physical oceanographic structures: southern elephant seals and mesoscale eddies east of Kerguelen Islands. Prog. Oceanogr. 87, 61–71. https://doi.org/10.1016/j.pocean.2010.09.025.

Dufau, C., Orsztynowicz, M., Dibarboure, G., Morrow, R., Le Traon, P.-Y., 2016. Mesoscale resolution capability of altimetry: present and future. J. Geophys. Res. Ocean 121, 4910–4927. https://doi.org/10.1029/2019JC014983.

Faghmous, J., Frenger, I., Yao, Y., Warmka, R., Lindell, A., Kumar, V., 2015. A daily global mesoscale ocean eddy dataset from satellite altimetry. Sci. Data 2 (1), 150028. https://doi.org/10.1038/sdata.2015.28.

Fang, F., Morrow, R., 2003. Evolution, movement and decay of warm-core Leeuwin Current eddies. Deep-Sea Res. II 50 (12), 2245–2261. https://doi.org/10.1016/S0967-0645(03)00055-9.

Gaube, P., Chelton, D.B., Strutton, P.G., Behrenfeld, M.J., 2013. Satellite observations of chlorophyll, phytoplankton biomass, and Ekman pumping in nonlinear mesoscale eddies. J. Geophys. Res. Ocean 118 (12), 6349–6370. https://doi.org/10.1002/2013JC009027.

Griffin, D.A., Middleton, J.H., 1986. Coastal-trapped waves behind a large continental shelf island, southern Great Barrier Reef. J. Phys. Oceanogr. 16 (10), 1651–1664. https://doi.org/10.1175/1520-0485(1986)016<1651:CTWBAL>2.0.CO;2.

Griffin, D.A., Middleton, J.H., Bode, L., 1987. The tidal and longer-period circulation of Capricornia, Southern Great Barrier Reef. Mar. Freshw. Res. 38 (4), 461–474. https://doi.org/10.1071/MF9870461.

Henson, S.A., Thomas, A.C., 2008. A census of oceanic anticyclonic eddies in the Gulf of Alaska. Deep Sea Res. I 55 (2), 163–176. https://doi.org/10.1016/j.dsr.2007.11.005.

Holbrook, N.J., Chan, P.S.-L., Venegas, S.A., 2005. Oscillatory and propagating modes of temperature variability at the 3–3.5- and 4–4.5-yr time scales in the upper Southwest Pacific Ocean. J. Clim. 18 (719–736), 1637–1639. https://doi.org/10.1175/JCLI-3286.1.

Holbrook, N.J., Goodwin, I.D., McGregor, S., Molina, E., Power, S.B., 2011. ENSO to multi-decadal time scale changes in East Australian current transports and Fort Denison sea level: oceanic Rossby waves as the connecting mechanism. Deep Sea Res. Part II Top. Stud. Oceanogr. 58, 547–558. https://doi.org/10.1016/j.dsr2.2010.06.007.

Jaine, F.R.A., Rohner, C.A., Weeks, S.J., Couturier, L.I.E., Bennett, M.B., Townsend, K.A., Richardson, A., 2014. Movements and habitat use of reef manta rays off eastern Australia: offshore excursions, deep diving and eddy affinity revealed by satellite telemetry. Mar. Ecol. Prog. Ser. 510, 73–86. https://doi.org/10.3354/meps10910.

Kleypas, J.A., Burrage, D.M., 1994. Satellite observations of circulation in the southern Great Barrier Reef, Australia. Int. J. Remote Sens. 15 (10), 2051–2063.

Liao, F., Wang, X.H., 2018. A study of low-frequency, wind-driven, coastal-trapped waves along the southeast coast of Australia. J. Phys. Oceanogr. 48 (2), 301–316. https://doi.org/10.1175/JPO-D-17-00 46.1.

Liu, Y., Dong, C., Guan, Y., Chen, D., McWilliams, J., Nencioli, F., 2012. Eddy analysis in the subtropical zonal band of the North Pacific Ocean. Deep Sea Res. I 68, 54–67. https://doi.org/10.1016/j.dsr.2012.06.001.

Mao, Y., Luick, J.L., 2014. Circulation in the southern Great Barrier Reef studied through an integration of multiple remote sensing and in situ measurements. J. Geophys. Res. Ocean 119 (3), 1621–1643. https://doi.org/10.1002/2013JC009397.

Müller, V., Kieke, D., Myers, P.G., Pennelly, C., Mertens, C., 2017. Temperature flux carried by individual eddies across 47° N in the Atlantic Ocean. J. Geophys. Res. Ocean 122 (3), 2441–2464. https://doi.org/10.1002/2016JC012175.

Nencioli, F., Dong, C., Dickey, T., Washburn, L., McWilliams, J.C., 2010. A vector geometry–based eddy detection algorithm and its application to a high-resolution numerical model product and high-frequency radar surface velocities in the Southern California Bight. J. Atmos. Ocean. Technol. 27 (3), 564–579. https://doi.org/10.1175/2009JTECHO725.1.

Okubo, A., 1970. Horizontal dispersion of floatable particles in the vicinity of velocity singularities such as convergences. Deep-Sea Res. Oceanogr. Abstr. 17 (3), 445–454. https://doi.org/10.1016/0011-7471(70)90059-8.

Peaven, P., 2011. Simple Ocean Eddy Detection Tools. https://sourceforge.net/p/eddydetect/code/HEAD/tree/.

Ridgway, K.R., Godfrey, J.S., 1997. Seasonal cycle of the East Australian current. J. Geophys. Res. Ocean 102 (C10), 22921–22936. https://doi.org/10.1029/97JC00227.

Ridgway, K., Hill, K., 2009. The East Australian Current. In A Marine Climate Change Impacts and Adaptation Report Card for Australia 2009 (E.S. Poloczanska, A.J. Hobday A.J. Richardson), NCCARF Publication 05/09, ISBN 978-1-921609-03-9.

Sadarjoen, I.A., Post, F.H., 2000. Detection, quantification, and tracking of vortices using streamline geometry. Comput. Graph. 24 (3), 333–341. https://doi.org/10.1016/S0097-8493(00) 00029-7.

Sims, D., Quayle, V., 1998. Selective foraging behaviour of basking sharks on zooplankton in a small-scale front. Nature 393, 460–464. https://doi.org/10.1038/30959.

Tian, F., Wu, D., Yuan, L.M., Chen, G., 2020. Impacts of the efficiencies of identification and tracking algorithms on the statistical properties of global mesoscale eddies using merged altimeter data. Int. J. Remote Sens. 41 (8), 2835–2860. https://doi.org/10.1080/01431161. 2019.1694724.

Wang, G., Su, J., Chu, P.C., 2003. Mesoscale eddies in the South China Sea observed with altimeter data. Geophys. Res. Lett. 30 (21) https://doi.org/10.1029/2003GL018532.

Weeks, S.J., Bakun, A., Steinberg, C.R., Brinkman, R., Hoegh-Guldberg, O., 2010. The Capricorn Eddy: a prominent driver of the ecology and future of the southern Great Barrier Reef. Coral Reefs 29, 975–985. https://doi.org/10.1007/s00338-010-0644-z.

Weimerskirch, H., Le Corre, M., Jaquemet, S., Potier, M., Marsac, F., 2004. Foraging strategy of a top predator in tropical waters: great frigatebirds in the Mozambique Channel. Mar. Ecol. Prog. Ser. 275, 297–308. https://doi.org/10.3354/meps275297.

Weiss, J., 1991. The dynamics of enstrophy transfer in two-dimensional hydrodynamics. Physica. D 48 (2–3), 273–294. https://doi.org/10.1016/0167-2789(91)90088-Q.

Williams, S., Hecht, M., Petersen, M., Strelitz, R., Maltrud, M., Ahrens, J., Hlawitschka, M., Hamann, B., 2011. Visualization and analysis of eddies in a Global Ocean simulation. Comput. Graph. Forum. 30, 991–1000. https://doi.org/10.1111/j.1467-8659.2011.01948.x.

Woodhead, P.M.J., 1970. Sea-surface circulation in the southern region of the Great Barrier Reef, spring 1966. Mar. Freshw. Res. 21 (2), 89–102. https://doi.org/10.1071/MF9700089.

Woodworth, P.A., Schorr, G.S., Baird, R.W., Webster, D.L., 2012. Eddies as offshore foraging grounds for melon-headed whales (Peponocephala electra). Mar. Mamm. Sci. 28, 638–647. https://doi.org/10.1111/j.1748-7692.2011.00509.x.

Xie, S., Huang, Z., Wang, X.H., 2021. Remotely sensed seasonal shoreward intrusion of the East Australian current: implications for coastal ocean dynamics. Remote Sens. 13, 854. https://doi.org/10.3390/rs13050854.

Yang, H., Lohmann, G., Wei, W., Dima, M., Ionita, M., Liu, J., 2016. Intensification and poleward shift of subtropical western boundary currents in a warming climate. J. Geophys. Res. Ocean 121, 4928–4945. https://doi.org/10.1002/2015JC011513.

Yang, H., Lohmann, G., Krebs-Kanzow, U., Ionita, M., Shi, X., Sidorenko, D., Gong, X., Chen, X., Gowan, E.J., 2020. Poleward shift of the major ocean gyres detected in a warming climate. Geophys. Res. Lett. 47 https://doi.org/10.1029/2019GL085868 e2019GL085868.

Yi, J., Du, Y., He, Z., Zhou, C., 2014. Enhancing the accuracy of automatic eddy detection and the capability of recognizing the multi-core structures from maps of sea level anomaly. Ocean Sci. 10 (1), 39–48. https://doi.org/10.5194/os-10-39-2014.